1 Introduction

Consider a supersonic flow over a thin flat plate of length L. Due to the viscous effects of the plate, a boundary layer will form from the leading edge of the plate. The presence of the boundary layer induces a shock wave, as seen in Figure 1

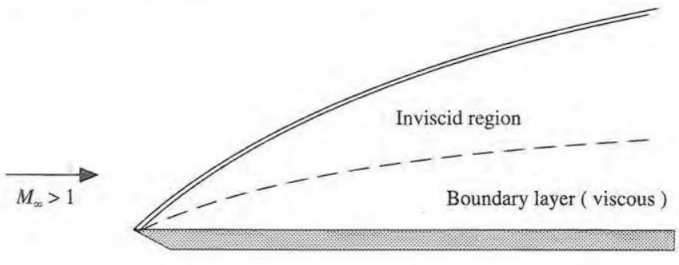

Figure 1: Boundary layer and shock wave

Despite the simplistic geometry, this flow possesses quite complex mechanics. Capturing the features of this flow numerically poses quite a challenge, but can be done through explicit finite difference calculations using MacCormack's method.

1.1 Governing Equations

Before discussing the numerical method, we must first understand the governing equations. This flow is governed by the 2D compressible Navier-Stokes equations. Assuming no outside body forces and no volumetric heating, the 2D Navier-Stokes equations are as follows:

$$\frac{\partial \rho}{\partial t} + \frac{\partial}{\partial x}(\rho u) + \frac{\partial}{\partial y}(\rho v) = 0 \tag{1}$$

$$\frac{\partial}{\partial t}(\rho u) + \frac{\partial}{\partial x}(\rho u^2 + p - \tau_{xx}) + \frac{\partial}{\partial y}(\rho uv - \tau_{yx}) = 0 \tag{2}$$

$$\frac{\partial}{\partial t}(\rho v) + \frac{\partial}{\partial x}(\rho uv - \tau_{xy}) + \frac{\partial}{\partial y}(\rho v^2 + p - \tau_{yy}) = 0 \tag{3}$$

$$\begin{aligned}\frac{\partial}{\partial t}(E_t) + \frac{\partial}{\partial x}((E_t + p)u + q_x - u\tau_{xx} - v\tau_{xy}) \\ + \frac{\partial}{\partial y}((E_t + p)v + q_y - u\tau_{yx} - v\tau_{yy}) = 0\end{aligned} \tag{4}$$

where Equation 1 is the continuity equation, Equations 2 and 3 are the momentum equations, and Equation 4 is the energy equation. Above, E_t is the total energy per unit volume, given by the sum of kinetic and internal energy e:

$$E_t = \rho(e + \frac{u^2 + v^2}{2}) \tag{5}$$

The stresses τ are given by:

$$\tau_{xx} = -\frac{2}{3}\mu(\frac{\partial u}{\partial y} + \frac{\partial v}{\partial x}) + 2\mu\frac{\partial u}{\partial x} \tag{6}$$

$$\tau_{xy} = \tau_{yx} = \mu(\frac{\partial u}{\partial y} + \frac{\partial v}{\partial x}) \tag{7}$$

$$\tau_{yy} = -\frac{2}{3}\mu(\frac{\partial u}{\partial y} + \frac{\partial v}{\partial x}) + 2\mu\frac{\partial v}{\partial y} \tag{8}$$

and the components of the heat flux vector q are:

$$\dot{q_x} = -k\frac{\partial T}{\partial x} \tag{9}$$

$$\dot{q_y} = -k\frac{\partial T}{\partial y} \tag{10}$$

Hear we have 5 equations and 8 unknowns: ρ, u, v, p, T, e, μ and k. Hence to close the system, we introduce the following 4 equations via some assumptions:

1. Assuming a perfect gas, we have the equation of state

$$p = \rho RT \tag{11}$$

2. If we assume air is calorically perfect, then

$$e = c_v T \tag{12}$$

where c_v is the specific heat of air at constant volume.

3. Further with the assumption of a calorically perfect gas, we have Sutherland's Law, which states

$$\mu = \mu_0(\frac{T}{T_0})^{3/2}\frac{T_0 + 110}{T + 110} \tag{13}$$

where μ_0 and T_0 are reference values for air at sea level.

4. If the Prandtl number is assumed to be constant (approximately 0.71 for callorically perfect air), then we have

$$\text{Pr} = 0.71 = \frac{\mu c_p}{k} \tag{14}$$

where c_p is the specific heat of air at constant pressure.

Now that the system is closed, we can write it in its conservative form

$$\frac{\partial U}{\partial t} + \frac{\partial E}{\partial x} + \frac{\partial F}{\partial y} = 0 \tag{15}$$

where U, E, and F are the conservative variables given in vector form as:

$$U = \begin{cases} \rho \\ \rho u \\ \rho v \\ E_t \end{cases} \tag{16}$$

$$E = \begin{cases} \rho u \\ \rho u^2 + p - \tau_{xx} \\ \rho uv - \tau_{xy} \\ (E_t + p)u - u\tau_{xx} - v\tau_{xy} + q_x \end{cases} \tag{17}$$

$$F = \begin{cases} \rho v \\ \rho uv - \tau_{xy} \\ \rho v^2 + p - \tau_{yy} \\ (E_t + p)v - u\tau_{xy} - v\tau_{yy} + q_y \end{cases} \tag{18}$$

so that now if we numerically solve Equation 15 for the conservative variables, we can then find the desired primitive variables.

2 Numerical Method

2.1 MacCormack's Method

We can numerically solve the conservative governing equations using MacCormack's method, which involves computing a "predictor" solution, followed by a "corrected" solution. Consider a numerical grid enumerated by i in the x-direction and j in the y-direction. First we rewrite Eq. 15 as

$$\frac{\partial U}{\partial t} = -\frac{\partial E}{\partial x} - \frac{\partial F}{\partial y} \tag{19}$$

Then through a Taylor expansion in time, we see that

$$U_{i,j}^{t+\Delta t} = U_{i,j}^{t} + (\frac{\partial U}{\partial t})_{av} \Delta t \tag{20}$$

where U is assumed to be known at time t. Here $(\partial U/\partial t)_{av}$ is a time step average from t to $t + \Delta t$, given by

$$(\frac{\partial U}{\partial t})_{av} = \frac{1}{2}((\frac{\partial U}{\partial t})_{i,j}^{t} + (\frac{\partial \bar{U}}{\partial t})_{i,j}^{t+\Delta t}) \tag{21}$$

where the overline denotes the predicted solution. The steady state solution can be computed via the following algorithm for each time step:

1. Compute Δt for the current time step. Time step sizes must change to ensure stability conditions are satisfied (see Sec. 2.2).

2. Compute the predicted values $\bar{U}$ using the values of E and F via forward finite difference:

$$\bar{U}_{i,j}^{t+\Delta t} = U_{i,j}^{t} - \frac{\Delta t}{\Delta x}(E_{i+1,j}^{t} - E_{i,j}^{t}) - \frac{\Delta t}{\Delta y}(F_{i,j+1}^{t} - F_{i,j}^{t}) \tag{22}$$

3. Compute the predicted values $\bar{E}$ and $\bar{F}$ using $\bar{U}$.

4. Compute the numerical solution U using corrector terms $\bar{E}$ and $\bar{F}$ via backward difference:

$$U_{i,j}^{t+\Delta t} = \frac{1}{2}[U_{i,j}^{t} + \bar{U}_{i,j}^{t+\Delta t} - \frac{\Delta t}{\Delta x}(\bar{E}_{i,j}^{t+\Delta t} - \bar{E}_{i-1,j}^{t+\Delta t}) - \frac{\Delta t}{\Delta y}(\bar{F}_{i,j}^{t+\Delta t} - \bar{F}_{i,j-1}^{t+\Delta t})] \tag{23}$$

This process is repeated until the desired steady-state solution is reached.

To maintain second order accuracy, the x-derivative terms of E are computed in the direction opposite to which was used for $\partial E/\partial x$ (e.g. since we compute the predictor solution using forward difference in Eq 22, the x-derivative terms of E must be computed using backward difference and the y-derivative terms must be computed using a central difference). Similarly, the y-derivative terms of F are computed in the opposite direction which was used for $\partial F/\partial y$, and the x-derivative terms are computed using a central difference.

After each predictor/corrector step, we can decode U to obtain the corresponding primitive variables using the equations below:

$$\rho = U_1 \qquad u = \frac{U_2}{U_1} \qquad v = \frac{U_3}{U_1} \qquad E_t = U_4$$

$$e = \frac{U_4}{U_1} - \frac{u^2 + v^2}{2} \qquad T = \frac{e}{c_v} \qquad p = \rho R T \qquad k = \frac{\mu c_p}{\mathrm{Pr}}$$

2.2 Step Size Calculations

Denote by N the number of desired grid points in the x and y direction. Given the plate length L, we can compute the x step size by

$$\Delta x = \frac{L}{N-1} \tag{24}$$

To fully capture the shock wave in the solution, we need to choose a sufficient step size in the y direction. From the Blasius solution of the flow past a flat plate, we determine that the vertical length of the domain must be at least 5 times the boundary layer thickness δ given by

$$\delta = \frac{5L}{\sqrt{\mathrm{Re}}} \tag{25}$$

Thus the step size in the y direction is

$$\Delta y = \frac{5\delta}{N-1} \tag{26}$$

To ensure stability, the time step Δt may change in each iteration. We compute Δt in each iteration using the local velocities, sound speed, viscosity, and density in the following way:

$$(\Delta t_{CFL})_{i,j} = \Big[\frac{|u_{i,j}|}{\Delta x} + \frac{|v_{i,j}|}{\Delta y} + a_{i,j}\sqrt{\frac{1}{\Delta x^2} + \frac{1}{\Delta y^2}} + 2\nu_{i,j}(\frac{1}{\Delta x^2} + \frac{1}{\Delta y^2})\Big]^{-1} \tag{27}$$

where

$$\nu_{i,j} = \max\Big[\frac{(4/3)\mu_{i,j}(\gamma\mu_{i,j}/\text{Pr})}{\rho_{i,j}}\Big] \tag{28}$$

$$\Delta t = \min[K(\Delta t_{CFL})_{i,j}] \tag{29}$$

for $0.5 \leq K \leq 0.8$. Here K serves as a "fudge factor", rather as an analogue to the CFL number which guarantees stability of the method under certain conditions.

3 Numerical Results

As mentioned in Section 1, we are modeling a supersonic flow over a flat plate. We assume the plate is of length $L = 0.00001$m and the inflow is air at sea level moving at Mach 4, with reference viscosity $\mu_0 = 1.7894 \times 10^{-5}$kg/(m-s) and a reference temperature $T_0 = 288.15$K, and we assume the temperature of the plate is constant at $T_w = T_0$. We assume the free stream pressure of air at sea level to be $p_0 = 10131$Pa and a heat capacity ratio $\gamma = 1.4$. We will conduct two numerical experiments, one with a domain limited in the x direction to the length of the plate, and another with a domain extended past the ends of the plate. In both cases, we will discritize the domain with $N_x = N_y = 71$ points in each direction, using i to denote the x direction and j to denote the y direction.

3.1 Limited Domain

We need to prescribe initial conditions throughout the entire grid at $t = 0$ and boundary conditions along $(i, 1)$, (i, N_y), $(1, j)$, and (N_x, j). For the initial conditions, we assume the flow parameters take their free stream values at each (i, j) except in the following cases (see Figure 2).

Case 1: At the leading edge of the plate $(1, 1)$, no-slip is enforced (i.e. $u_{1,1} = v_{1,1} = 0$) and the temperature and pressure are assumed to be their free stream values.

Case 2: At the inflow positions $(1, j)$ not including the leading edge, and along the top of the domain (i, N_y), we assume x velocity, temperature, and pressure are the free stream values, and y velocity is 0.

Case 3: Along the edge of the plate $(i, 1)$ not including the leading edge, no-slip is enforced, and the temperature of the plate is given as T_w. The pressure along the plate is extrapolated from the interior pressure by $p(i, 1) = 2p(i, 2) - p(i, 3)$.

Case 4 At the outflow positions (N_x, j) not including the plate, we extrapolate the velocities, temperature, and pressure as seen in Case 3.

Since these boundary conditions are extrapolated from the interior, we need to compute them in every time step twice, once before the initial computation, and again for the predicted primitive variables.

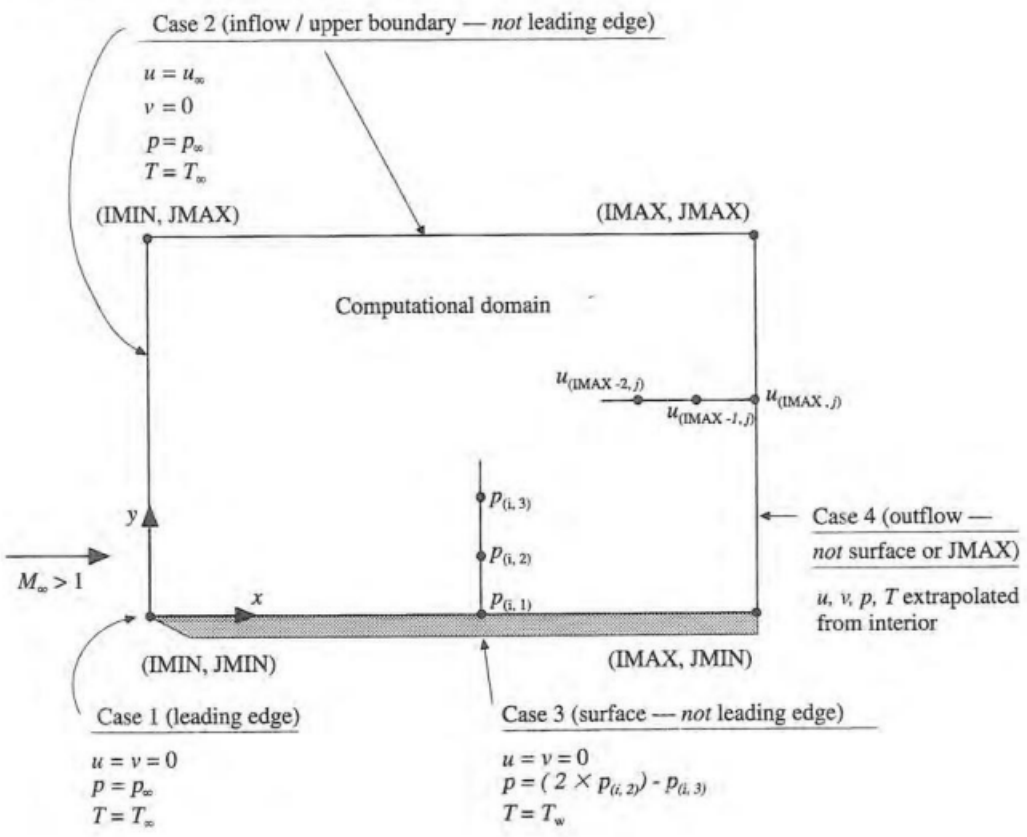

Figure 2: Boundary conditions of the method

In Figure 3a we have the resulting steady state temperature field of the supersonic flow, and in Figure 3b we have the Mach number field of the flow. From the temperature field, we can see both the shock wave and boundary layer present, both eminating from the leading edge of the plate. The shock wave is the upper contour line $T \approx 300$, while the boundary layer remains closer to the plate beneath the $T \approx 420$ contour. We can also visualize the shock wave through the pressure field (Figure 4a) and the density field (Figure 4b). The shock wave represents a discontinuous jump in pressure and density, which is clearly seen in these contours.

We also plot the shear stress τ and heat transfer q along the surface of the plate in Figures 5a and 5b respectively. The shear stress and heat transfer along the plate are given by

$$\tau = \mu \frac{\partial u}{\partial y}\Big|_{y=0} \qquad\qquad q = \kappa \frac{\partial T}{\partial y}\Big|_{y=0}$$

where the derivatives are computed using a 3-point second order accuruate forward difference:

$$\frac{df}{dy} = \frac{-3f_i + 4f_{i+1} - f_{i+2}}{2\Delta y} \tag{30}$$

In Figure 3b we have a semilogy plot of the residual errors of the conservative variables U_1-U_4 (the residuals were computed using the Frobinius norm $\sqrt{A^T A}$ at each iteration step). From this plot, we can see that each of the conservative variables converges at approximately the same

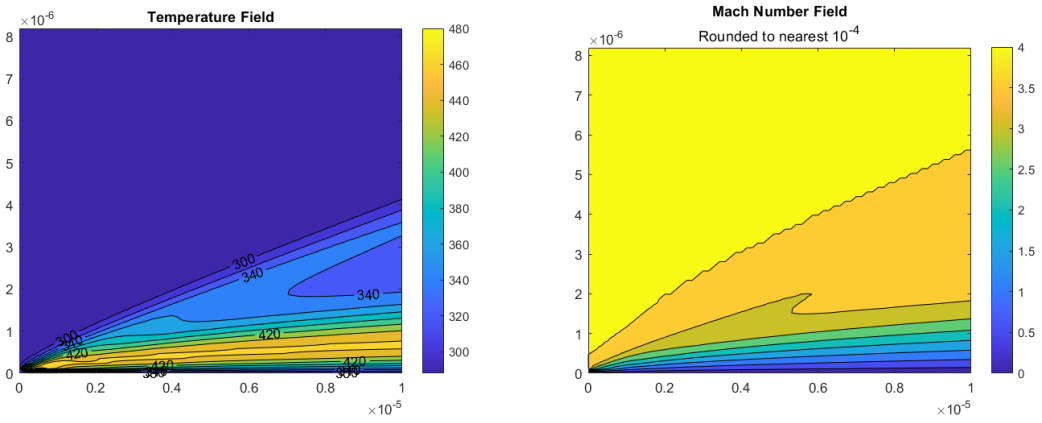

(a) (b)

Figure 3: (a) Temperature field and (b) Mach number field of the supersonic flow.

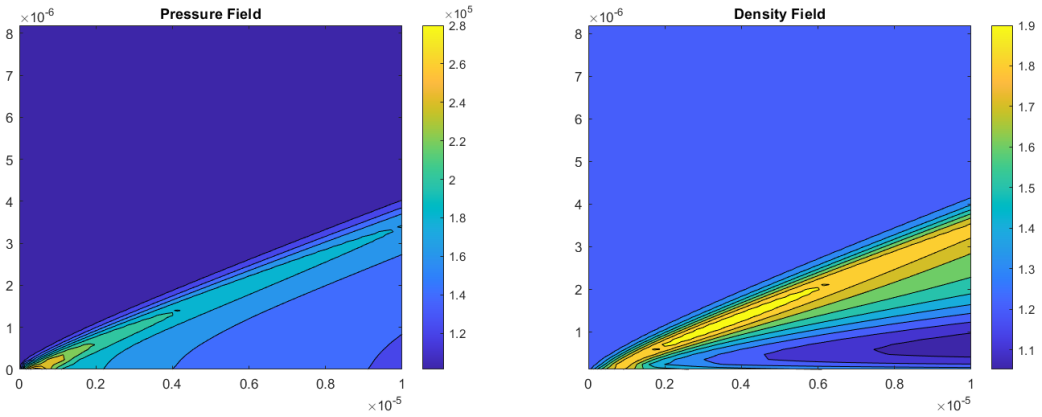

(a) (b)

Figure 4: (a) Pressure field and (b) density field of the supersonic flow.

rate, with U_4 only reaching $\approx 10^{-8}$. The fact that convergence is determined predominately by U_4 makes some sense when we consider that this variable is the total energy of the system E_t. As the steady state solution should be an energy minimizing solution, it seems likely that the energy of the system would determine the overall convergence of the method.

3.2 Extended Domain

Now we will extend the domain slightly past both ends of the plate, as well as doubling the grid points in both the x and y directions. We keep most of the parameters the same, except we now let $N_x = N_y = 141$, and define the grid such that the plate begins at $x = 0.2 \times 10^{-5}$ and ending at $x = 1.2 \times 10^{-5}$. We also double the length of the y domain to $10 \times \delta$.

To deal with this extended domain, we introduce symmetry boundary conditions along the bottom of the grid upstream and downstream the plate. In particular, we assume that the derivative normal $y =$ is 0. We can make use of the second order accurate forward difference from Eq 30 to

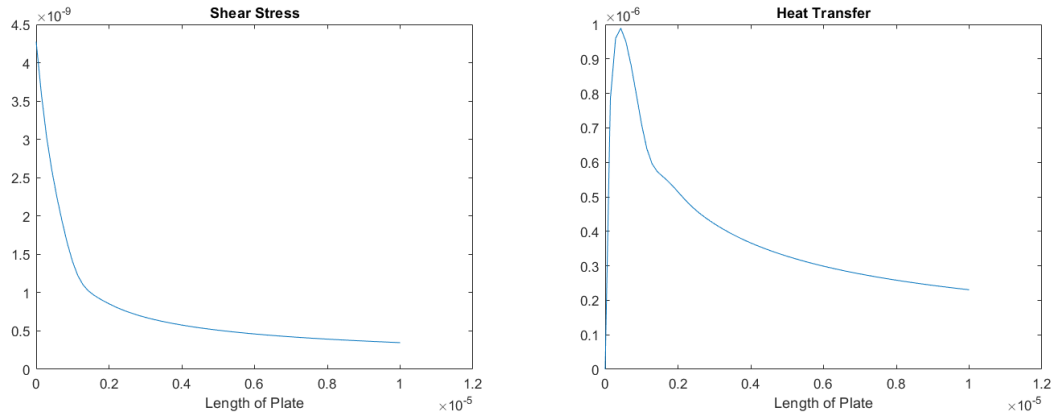

(a) (b)

Figure 5: (a) Shear stress and (b) Heat transfer along the surface of the plate.

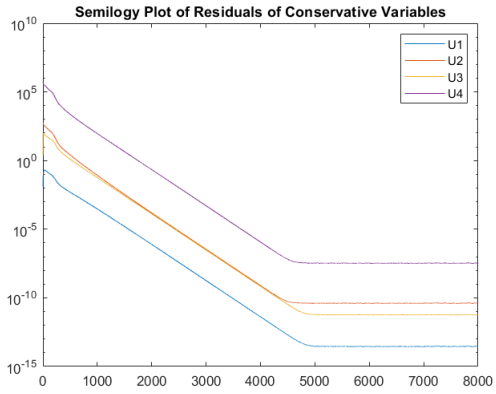

Figure 6: Semilogy plot of the residuals of the conservative variables versus the number of iterations.

approximate the values of u, p, and T along the bottom of the grid at $y = 0$ by setting the derivative to 0 and solving for f_i:

$$f_i = \frac{4f_{i+1} - f_{i+2}}{3} \tag{31}$$

Note that there is no need to approximate v as we assume the free stream y velocity to be 0.

Figure 7a denotes the resulting temperature field, along with the corresponding Mach number field in Figure 7b. As before, we can see the shock wave and boundary layer eminating from the leading edge of the plate. However, now we can see how the shock wave travels past the far edge of the plate, while the boundary layer dissipates relatively quickly past the far edge of the plate. Perhaps this shows how viscous effects in a supersonic flow are overpowered by the presence of the shock wave. We also plot the pressure field and density field in Figures 8a and 8b respectively. Again notice how the effects of the shock wave travel past the far edge of the plate without dissipating.

In Figures 9a and 9b we plot the shear stress and heat transfer along the surface of the plate respectively. We can integrate these curves over the length of the plate to compute the total drag

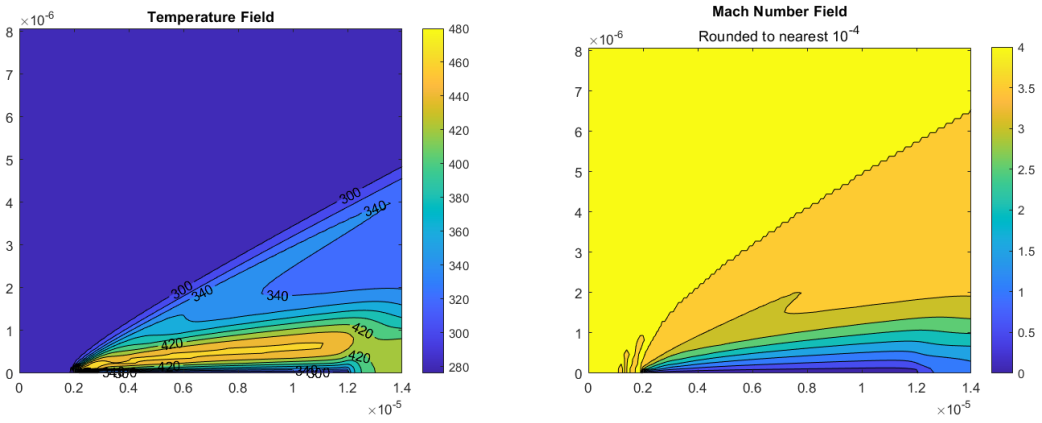

(a) (b)

Figure 7: (a) Temperature field and (b) Mach number field of the flow computed over the extended domain.

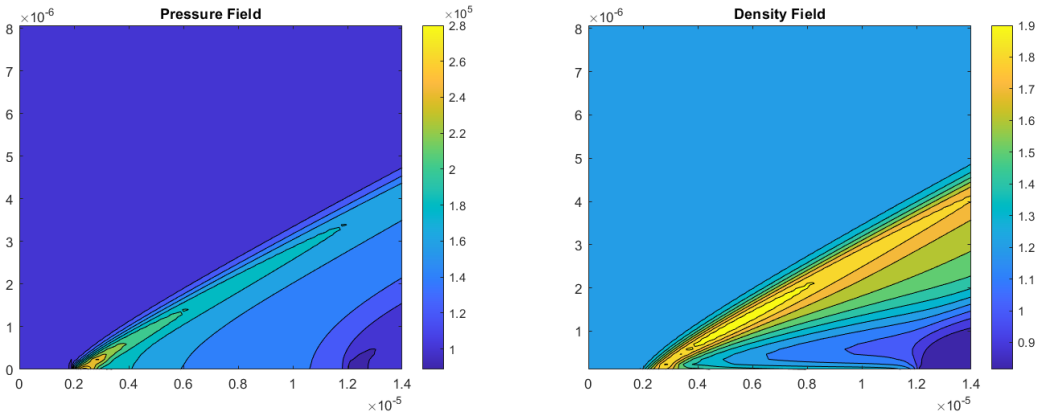

(a) (b)

Figure 8: (a) Pressure field and (b) density field of the supersonic flow computed over the extended domain.

and total heating rate along the plate surface:

$$\text{Drag} : D = 7.3616 \times 10^{-08}\text{N} \qquad \text{Heat Rate} : Q = 3.9461 \times 10^{-05}\text{W}$$

It is interesting that the drag along the plate is nonzero, as the initial flow is completely parallel to the plate. This is perhaps due to the viscous effects causing a shear flow within the boundary layer. Although we can see that most of the shear stress occurs at the leading edge of the plate, which intuitively makes sense.

We also plot the semilogy of the residuals of the conservative variables in Figure 10. The overall convergence of the method remains the same, as to be expected. However, of course, the total computation time of the method is significantly higher (about 20 times) due to the vastly increased number of grid points.

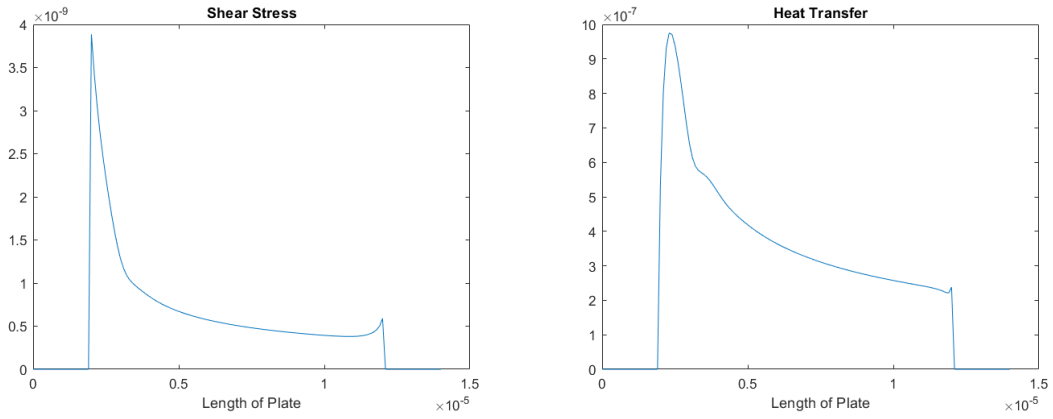

(a) (b)

Figure 9: (a) Shear stress and (b) Heat transfer along the surface of the plate.

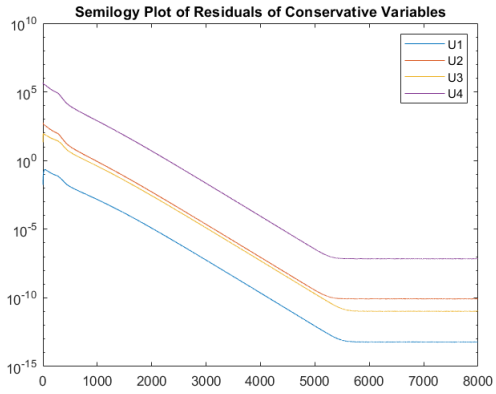

Figure 10: Semilogy plot of the residuals of the conservative variables versus the number of iterations computed over the extended domain.

4 Conclusions

In this project, we have successfully modeled a supersonic flow past a flat plate via the compressible Naveir-Stokes equations. Using MacCormack's method, we found the steady state solution of the flow across both a limited and an extended domain. The resulting temperature and Mach number fields give valuable insight into the flow. Analytically, we expected the presence of both a boundary layer and a shock wave, but the numerical solution helps to visualize the separation of the two. From Figures 3 and 7, we can see how both the shock wave and boundary layer eminate from the leading edge of the plate, and how they separate as the flow travels farther past the plate. Through the extended domain in Figure 7a, we can also see how the boundary layer dissipates quickly past the end of the plate, while the shock wave continues. Through the residuals in Figures 6 and 10, we can see that the convergence to the steady state solution is dependent on the minimization of the total energy of the system, which validates the numerical findings of the experiments.